Quantifying the effect of mineralogical composition on mechanical properties of Montney siltstone using micro-indentation tests and SEM-EDS analysis

Huan Yu, Wenbo Zheng, Jianhui Zhou
School of Engineering – University of Northern British Columbia, Prince George, British Columbia, Canada
Albert Cui
AGAT Laboratory, Calgary, Alberta, Canada

ABSTRACT
Rock mechanical properties are important input parameters for designing drilling and recovering unconventional hydrocarbons from tight formations. Mineralogical composition of tight reservoir rocks can change significantly along depths and laterally for a tight formation, which affects their rock mechanical properties. While traditional expensive compressional tests on standard-sized rock samples can provide bulk rock mechanical parameters, but little insights on its relationship to mineralogical composition at a micro-scale. Using siltstone samples from the Montney gas play as an example, this paper aims to quantify the influence of rock mineralogical composition on their mechanical properties using micro-indentation tests and SEM-EDS analysis. Nine disk-shaped siltstone samples were made from Montney cores drilled in NE BC and nine micro-indentation tests were conducted on each rock sample. Using the obtained indentation force-displacement curves, the local Young's modulus and Brinell hardness at each indent were determined. Then the scanning electron microscopy (SEM) and energy-dispersive spectroscopy (EDS) analyses of the indentation sites were conducted to determine the mineralogical texture and chemical/elemental distributions locally for each indentation. Based on the known mineral types from X-ray diffraction analysis (XRD), the chemical distributions at each local indent were used to determine the quantitative mineralogical composition at each indent site using a least-square method. The determined local mineral composition is analyzed against the local Young's modulus and hardness for each indentation, leading to an improved understanding of quartz+feldspar, clay minerals, and carbonate in affecting rock mechanics properties in tight formations.

RÉSUMÉ
Les propriétés mécaniques de la roche sont des paramètres d'entrée importants pour la conception du forage et la récupération des hydrocarbures non conventionnels des formations étanches. La composition minéralogique des roches réservoirs étanches peut changer de manière significative le long des profondeurs et latéralement pour une formation étanche, ce qui affecte leurs propriétés mécaniques. Alors que les tests de compression traditionnels coûteux sur des échantillons de roche de taille standard peuvent fournir des paramètres mécaniques de roche en vrac, mais peu d'informations sur sa relation avec la composition minéralogique à une micro-échelle. En utilisant des échantillons de siltstone de la zone gazière de Montney comme exemple, cet article vise à quantifier l'influence de la composition minéralogique des roches sur leurs propriétés mécaniques à l'aide de tests de micro-indentation et d'analyse SEM-EDS. Neuf échantillons de siltstone en forme de disque ont été prélevés à partir de carottes de Montney forées dans le NE de la Colombie-Britannique et neuf tests de micro-indentation ont été effectués sur chaque échantillon de roche. En utilisant les courbes force-déplacement d'indentation obtenues, le module de Young local et la dureté Brinell à chaque indentation ont été déterminés. Ensuite, les analyses par microscopie électronique à balayage (SEM) et spectroscopie à dispersion d'énergie (EDS) des sites d'indentation ont été menées pour déterminer la texture minéralogique et les distributions chimiques/élémentaires localement pour chaque indentation. (XRD), les distributions chimiques à chaque empreinte locale ont été utilisées pour déterminer la composition minéralogique quantitative à chaque site d'empreinte en utilisant une méthode des moindres carrés. La composition minérale locale déterminée est analysée par rapport au module de Young local et à la dureté pour chaque empreinte, conduisant à une meilleure compréhension du quartz + feldspath, des minéraux argileux et du carbonate affectant les propriétés mécaniques des roches dans les formations étanches.

1 INTRODUCTION

The production of natural gas in unconventional formations has significantly increased due to the development of horizontal drilling and multi-stage hydraulic fracturing in the past two decades (Cheng et al. 2022; Sharma et al. 2019). The Montney unconventional gas play in northeast British Columbia has become the largest gas producer in the province and two-thirds horizontal of wells stimulated with hydraulic fracture have targeted the Montney formation with abundant silt-rich mudstone (siltstone) (Rivard et al. 2014; Vishkai et al. 2017). The fracture network created by hydraulic fracturing is highly related to the rock mechanical properties of targeted formations (Rivard et al., 2014), of which the rock mineralogy is an important influence factor (Cheng et al. 2022). The localized rock mechanical properties also affect the embedment of

proppants pumped into fractures, thus affecting the fracture conductivity (Zheng et al. 2019). Hence, studying the linkage between rock mechanical parameters and mineralogy at a micro-scale is necessary.

The micro-indentation test aimed to determine the hardness and elastic modulus of thin films and small solid samples by measuring the indentation depth with the increased indentation force with an indenter (Poon et al. 2008). Compared with the traditional compressional tests, the indenter can apply forces on a small area to create high localized stress that enables measuring the localized mechanical properties at a micro-scale (Kasyap et al. 2021; Song et al. 2022). Meanwhile, scanning electron microscopy (SEM) can obtain high-resolution micro-morphologies of sample surfaces with great precision by scanning samples with a narrowly focused high-energy electron beam to obtain various physical information through the interactions between the beam and the rock surface (Fandrich et al. 2007). The energy-dispersive spectroscopy (EDS) system is attached to the SEM instrument to enable the chemical analysis of the scanned area (Akkaş et al. 2015; Meyer et al. 2013).

This research investigated nine disk-shaped siltstone samples prepared from Montney cores drilled at a depth between 2068.29 m and 2337.39 m in Northeast British Columbia. Nine micro-indentation tests were conducted on each rock sample to obtain indentation force-displacement curves. The local Young's modulus and hardness at each indent were determined using Oliver and Pharr's method (Oliver & Pharr, 2004) from the force-displacement curves. After the indentation tests, SEM and EDS analyses were used to determine the localized microstructure of mineralogical grains and their chemical elements at indentation locations. The weight percentages of chemical elements were used to calculate the mineral compositions by a least-square method. Finally, the influence of rock's chemical elements and mineralogical compositions on their mechanical properties is discussed.

2 MATERIALS AND METHODS

2.1 Sample preparations

Nine samples were prepared from the drilling core of well #28232 (HZ TOWN C-031-H/094-B-09), located in the Lower Triassic Montney play in Northeast British Columbia. The samples were drilled parallel to the slab face of the two-third cores along the horizontal direction. The samples are disk-shaped with a nominal 25.4 mm diameter and 25.4 mm length. The disk samples were coated with an epoxy resin ring and the end surfaces were polished using the Buehler AutoMet 250 for the micro-indentation test.

The measured core depths (MD) are from 2068.29 m to 2337.39 m. For comparison, cores were selected from two formations: the Doig formation (2030.16 m to 2073.36 m) and the Montney formation (2073.35 m to 2379.55 m). Detailed information on the samples is listed in Table 1.

Table 1. Detailed information on samples

No.	Measured Depth (m)	Formation
S1	2068.29	Doig Formation
S2	2068.55	Doig Formation
S3	2068.76	Doig Formation
S4	2265.85	Montney Formation
S5	2336.04	Montney Formation
S6	2336.08	Montney Formation
S7	2336.21	Montney Formation
S8	2336.37	Montney Formation
S9	2337.39	Montney Formation

2.2 Experiments

2.2.1 Micro-indentation test

Micro-indentation tests were performed using a Nanovea M1 Indentation Instrument and the indenter tip is a spherical carbide tungsten ball with a diameter of 1 mm. For each sample, nine tests were conducted at nine different locations (L1 to L9) in a three by three grid shown in Figure 1.

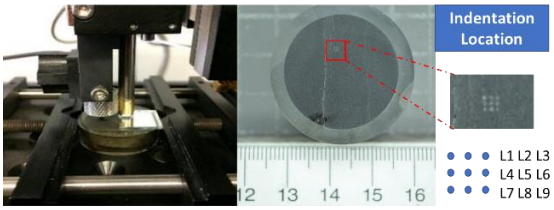

Figure 1. Indentation equipment (left), rock sample (middle) and tested locations (right) (modified from Zheng et al. 2019)

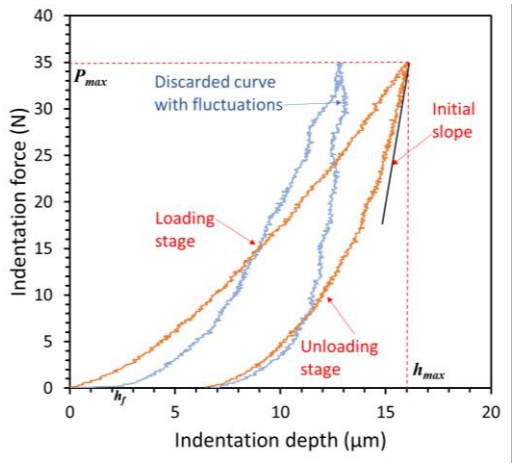

Figure 2. Typical indentation force vs. depth curves

The typical indentation force vs. indentation depth curve is shown in Figure 2. The indentation force was increased up to 35 N and then unloaded to 0 N, both with a constant rate of 17.5 N/min. However, the final indentation depth did not fully recover to zero after the unloading stage. This unrecoverable final depth is due to plastic deformation and is termed as plastic depth, whereas the difference between the maximum indentation depth and the plastic depth is termed as elastic depth. The curve of the unloading stage can be used to calculate the local typical mechanical properties, such as Young's modulus and hardness, which will be described in 2.3.1. Note that the results with significant fluctuations were discarded and not include in the analysis of this paper.

2.2.2 SEM and EDS analysis

In order to determine the localized microstructure of mineral grains and their elemental compositions, SEM and EDS analyses were performed on the nine indentation locations (L1 to L9) of each sample. Furthermore, to better understand the bulk properties of the sample as a whole, one additional scan was performed with SEM and EDS that covered a larger area to include the L1 to L9 locations, which is termed as L10. The electron images of the test locations were obtained with the Tescan Mira 3 XMU Scanning Electron Microscope employing a field emission gun, and elemental distributions were determined with the Oxford Instruments X-Max Energy Dispersive Spectrometer detector.

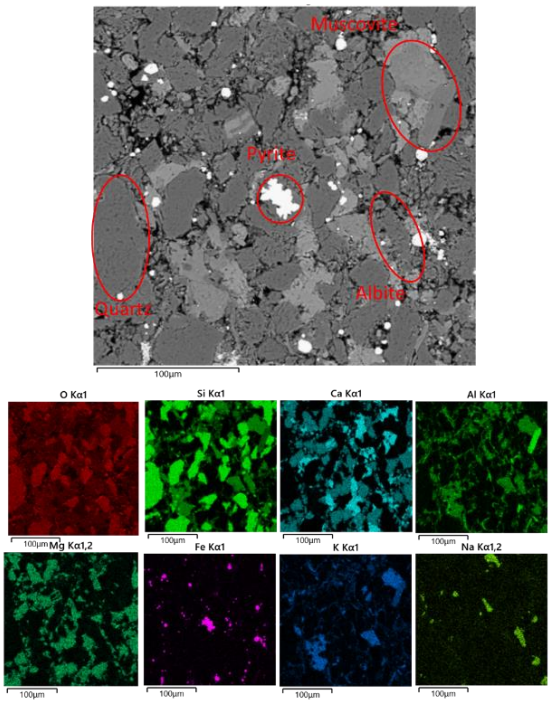

Figure 3. The electron image of SEM and elements layered images of EDS

As shown in Figure 3, the high-resolution SEM images show heterogeneous rock microstructure, and different colors of layered EDS images represent the distributions of chemical elements. With known chemical formulas of minerals and the element concentrations and distributions from the layered images of EDS at the same location canbe used to roughly determine the mineral type of grains on the SEM images. For example, common rock-forming minerals, quartz (SiO_2), Pyrite (FeS_2), Muscovite ($KAl_2(Si_3AlO_{10})(OH)_2$) , Albite ($NaAlSi_3O_8$) and these mineral grains are marked in Figure 3.

2.3 Methods

2.3.1 Conventional Mechanical Properties

The conventional mechanical properties of rock, Young's modulus and hardness, are obtained by the method proposed by Oliver and Pharr (Oliver & Pharr, 2004), which is termed the O-P method. This method assumed the recoverable depth during the unloading stage is elastic. Thus, the curve of indentation force (P) and indentation depth (h) of the unloading stage was selected for the analysis. The P-h curve is fitted with a power-law equation:

$$P = \alpha(h - h_f)^m \quad [1]$$

where α and m are fitting constants.

The contact stiffness (S) between the indenter tip and the tested material is determined by the initial slope of the P-h curve at the unloading stage:

$$S = dP/dh \quad [2]$$

The contact depth (h_c) between the indenter and sample can be calculated as:

$$h_c = h_{max} - \epsilon P_{max}/S \quad [3]$$

where P_{max} is the maximum force, h_{max} is the corresponding maximum depth with P_{max}, and ϵ is the constant depending on the geometry of the indenter. For the spherical indenter, ϵ is 0.75. Using h_c, the true contact projected area (A_c) between the indenter and sample can be calculated as:

$$A_c = \pi[r^2 - (r^2 - h_c)^2] \quad [4]$$

where r is the radius of the spherical indenter.

The hardness can be obtained as:

$$H = P_{max}/A_c \quad [5]$$

As the force also causes the elastic deformation of the indenter, hence, the effective Young's modulus (E_{eff}) presents the apparent Young's modulus between samples and indenter and is defined:

$$E_{eff} = \sqrt{\pi}S/2\beta\sqrt{A_c} \quad [6]$$

where β is the effective coefficient of all physical processes, which is 1.05 in this study (Oliver & Pharr, 2004).

Moreover, Young's modulus of the sample is calculated as:

$$1/E_{eff} = (1-v^2)/E + (1-v_i^2)/E_i \quad [7]$$

where v and E are the Poisson's ratio and Young's modulus of the sample while v_i and E_i are Poisson's ratio and Young's modulus of the indenter. In this study, v_i=0.31 and E_i=600 GPa are used for for the spherical indenter, and the v=0.25 is assumed for the tested samples.

2.3.2 Least-square Method

The overall weight percentages (wt%) of chemical elements in a rock sample are closely associated with the relative quantities of different minerals and the chemical formulas of each mineral. Hence, the weight proportions of minerals can be reversely calculated according to the overall weight distributions of chemical elements when the mineral types are known.

The least-square method is a regression analysis to approximate the solutions of overdetermined equations, which is shown as:

$$f(x) = \begin{pmatrix} C_{11} & \cdots & C_{1n} \\ \vdots & \ddots & \vdots \\ C_{m1} & \cdots & C_{mn} \end{pmatrix} \begin{pmatrix} x_1 \\ \vdots \\ x_n \end{pmatrix} - \begin{pmatrix} b_1 \\ \vdots \\ b_m \end{pmatrix} \quad [8]$$

In this study, $\|C\|$ is the weight percentage matrix of chemical elements derived from the chemical formula of minerals, $\|x\|$ is the relative weight of different types of minerals, and $\|b\|$ is the measured relative weight of chemical elements.

The results of X-ray diffraction (XRD) and X-ray fluorescence (XRF) of the tested samples are retrieved from reports of well #28232 in a database provided by the BC Oil and Gas Commission (British Columbia Oil and Gas Commission. 2013). The available data of depths from 2068 m to 2358 m is applied to verify the feasibility of the least-square method to calculate the weight percentage of minerals.

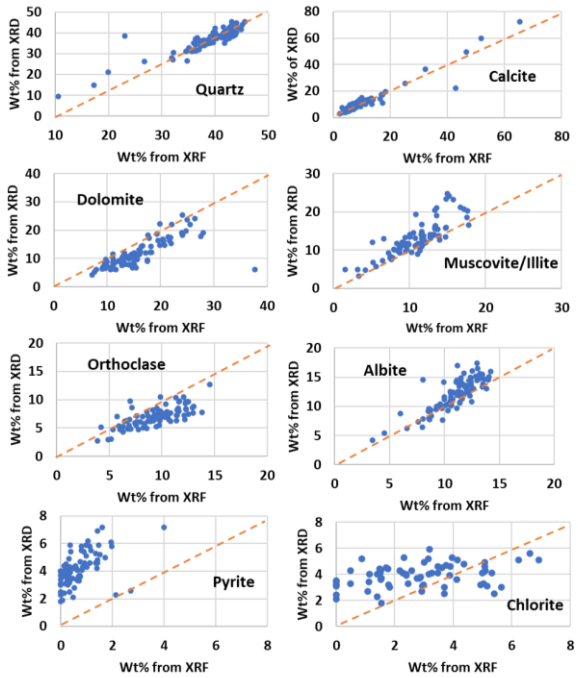

Figure 4. Comparison of the weight percentage of minerals between XRD and XRF

Table 2. Mineralogy of the tested samples and their chemical formulas

Mineral type	Chemical formula
Albite	$NaAlSi_3O_8$
Calcite	$CaCO_3$
Dolomite	$Ca(Mg_{0.67}Fe_{0.33})(CO_3)_2$
Muscovite/Illite	$KAl_2(Si_3AlO_{10})(OH)_2$
Orthoclase	$KAlSi_3O_8$
Pyrite	FeS_2
Quartz	SiO_2
Chlorite	$(Mg,Al)_6(Si,Al)_4O_{10}(OH)_8$

Although the mineral types and their chemical formula in this depth have been reported in the XRD data, some minerals may have slightly different chemical formulas. Therefore, the weight percentages of chemical elements obtained from XRD data were firstly compared with the XRF data, which satisfactorily verified the minerals' chemical formulas shown in Table 2.

According to Table 2, $\|C\|$ in Eq.(8) set was determined. $\|b\|$ was obtained from the weight percentage of chemical elements using the XRF data. The solution of $\|x\|$ was the weight percentage of the known mineral types. As shown in Fig. 4, the results showed good consistency between the predicted and measured major mineral components. The discrepancies between the predicted versus the lab-measured mineral weights are mostly in pyrite and chlorite, both of which constituted only a small proportion

of total weight. Therefore, the validated least-square method was used in this paper to predict the mineral compositions at local indentation sites using the SEM-EDS elemental composition results.

3 RESULTS

3.1 Young's Modulus and Hardness

Based on the results of unloading *P-h* indentation curves, Young's Modulus and hardness were determined using the O-P method. The determined Young's modulus and hardness for each sample in terms of their average value (Ave), standard deviation (Std) and the coefficient of deviation(Cv) are summarized in Table 3.

Table 3. Summary of Young's modulus and hardness

No.	No. of data set	Hardness (GPa)		Young's modulus (GPa)	
		Ave ± Std	Cv	Ave ± Std	Cv
S1	7	0.80±0.09	0.11	32.0±9.53	0.30
S2	8	0.94±0.06	0.07	36.2±2.2	0.06
S3	2	0.86±0.24	0.28	58.37±9.0	0.15
S4	8	0.88±0.10	0.11	19.5±3.4	0.17
S5	6	0.83±0.04	0.04	65.72±3.3	0.05
S6	4	1.11±0.16	0.15	92.5±14.1	0.15
S7	4	0.65±0.14	0.22	44.0±3.6	0.08
S8	1	0.88±0.00	0.00	58.8±0.0	0.00
S9	7	1.07±0.20	0.18	48.9±25.6	0.52
Total	47	0.90±0.17	0.19	45.3±23.1	0.51

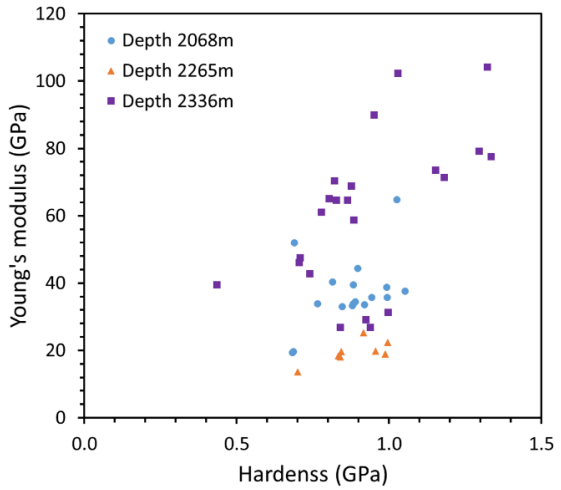

Figure 5. Young's modulus vs. hardness

Figure 5 shows raletionship between the local Young's modulus and hardness for the 47 data points of the nine samples at three core depths. The blue points present samples around 2068m from the Doig formation, and the orange triangles and purple squares present samples around 2265 m and around 2336 m respectively, and both are from the Montney formation. It shows that for samples from the same depth and formation, the values of Young's modulus and hardness of samples were relatively close to each other. Secondly, samples at two different depths from the Montney formation have different mechanical characteristics, that shallower samples at about 2265 m have lower Young's modulus than the samples from a greater depth (2336 m). Interestingly, Young's modulus of the samples from the Doig formation (2068 m) was higher than 2265 m but lower than 2336 m.

3.2 Localized Chemical Elements Distributions

The localized mineral chemical elements were obtained from SEM and EDS analysis. The bulk chemical element distributions of each rock sample are shown in Fig. 6.

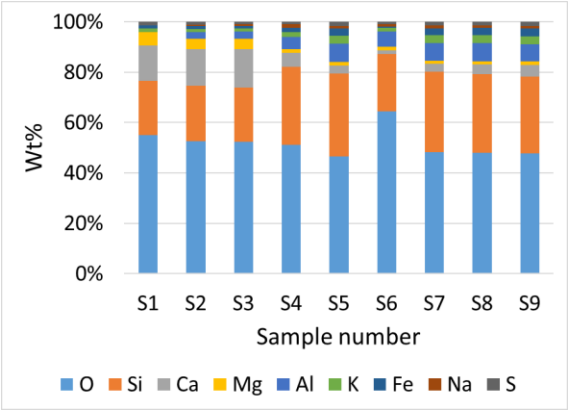

Figure 6. The overall weight percentage of chemical elements of nine rock samples

In Figure 6, it can be seen that Oxygen (O) accounts for the largest proportion, around 47.7%-64.4%, as most minerals contain O. Silicon (Si) is the second most abundant element, around 21.4%-32.7%, which is the main component of quartz and other silicates. Meanwhile, three samples (S1 to S3) from the Doig formation contain more calcium (Ca) than other samples from the Montney Formation, which means samples from the Doig formation might comprise more carbonate minerals than samples from the Montney Formation.

3.3 Localized Mineral Composition

The localized mineral compositions were determined by the least-square method in 2.3.2 based on chemical element distributions from the SEM-EDS analysis. Figure 7 depicts the weight percentage and types of minerals for all nine samples using the data from a larger scanning area, L10.

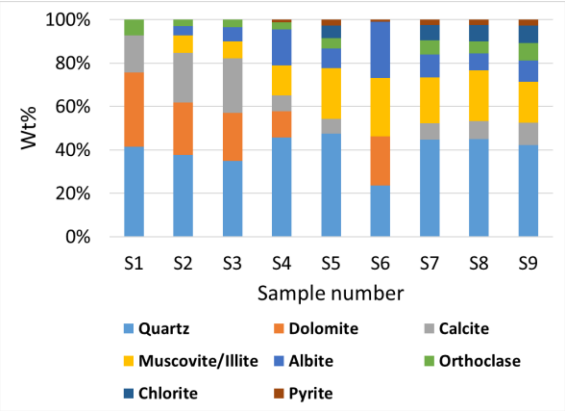

Figure 7. The calculated weight percentage of mineral composition for nine rock samples

The Figure 7 showed that except for S6, the quartz (SiO_2) accounted for the largest weight proportion for most samples, around 35.0%-45.7%. For samples S1 to S3 from the Doig formation, the carbonate minerals, dolomite ($Ca(Mg_{0.67}Fe_{0.33})(CO_3)_2$) and calcite ($CaCO_3$), constituted nearly 50% weight percentage, while dolomite accounted only for a small proportion in the samples from the Montney formation. In contrast, clay mineral muscovite/illite ($KAl_2(Si_3AlO_{10})(OH)_2$) from the Montney formation (S4 to S9) is higher than samples from the Doig formation.

The mineral compositions of S6 were different from others, as the weight percentage of quartz decreased while the weight percentage of muscovite/illite increased. The reason is that compared with other samples, there is a large proportion of O, around 65% for S6, and the relative proportion of Al is high as well, which is mainly associated with muscovite/illite with relatively lower proportion of Si, which is the main chemical element of quartz shown in Figure 6.

4 DISCUSSIONS

The Pearson correlation coefficient method is used to investigate the influence of the composition of chemical elements and minerals on the sample's Young's modulus and hardness. The P-values of the Pearson correlation coefficient range from 0 to 1; P less than 0.05 indicates a significant correlation between two groups of data. R is the correlation coefficient ranging from -1 to 1. Negative R values indicate the negative correlation and vice versa, while R = 0 means no correlation. The values of P and R were calculated in MATLAB.

4.1 Effect of Chemical Elements on Mechanical Properties

Figure 8 shows the correlations between mechanical properties and chemical elements, and their corresponding P-values and R coefficients are also listed. For the scatter plots, the horizontal axis is the weight percentage of elements ranging from 0 to 100%, and the vertical axis represents the values of hardness or Young's modulus.

The data points of some chemical elements with small weight were almost distributed along a vertical line, such as K, Na, and S, which means a small deviation of element content at the tested indentation sites. This results in lower P-values and R coefficients between these elements and rock's mechanical properties, which could be artificial. There are correlations between Young's modulus and Ca and Al, as both P-values of Ca are smaller than 0.05. According to the values of R, Ca is negatively correlated with Young's modulus while Al has a positive relationship. From the chemical formulas of minerals listed in Table 2, Ca is the main component of dolomite and calcite, while Al is the main component of albite, muscovite/Illite, orthoclase, and chlorite.

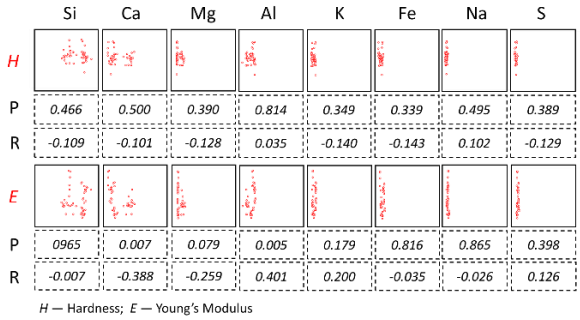

Figure 8. Scatter plots between mechanical properties and chemical elements and their P and R values

4.2 Effect of Minerals on Mechanical Properties

Figure 9 plots the rock mechanical properties with their minerals, and the P-values and R coefficients are also provided. For the scatter charts, the horizontal coordinate is the weight percentage of minerals ranging from 0 to 100%, and the vertical coordinate represents hardness and Young's modulus.

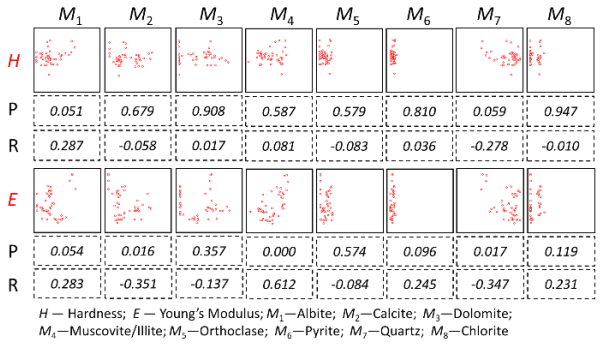

Figure 9. Scatter plots between mechanical properties and minerals and their P and R values

From Fig. 9, the data points of pyrite, orthoclase, and chlorite were distributed almost along a vertical line,

which indicates limited variation and low percentages, and their effect on hardness and Young's modulus can not be determined confidently. There is a positive correlation between hardness and albite with a P-value = 0.051 and R = 0.287. Furthermore, calcite and quartz showed a negative correlation with Young's modulus, and there was a positive correlation between Young's modulus and muscovite/illite. Meanwhile, the correlations of muscovite/illite and calcite with hardness and Young's modulus are consistent with the correlations of chemical elements with hardness and Young's modulus that were discussed in 4.1.

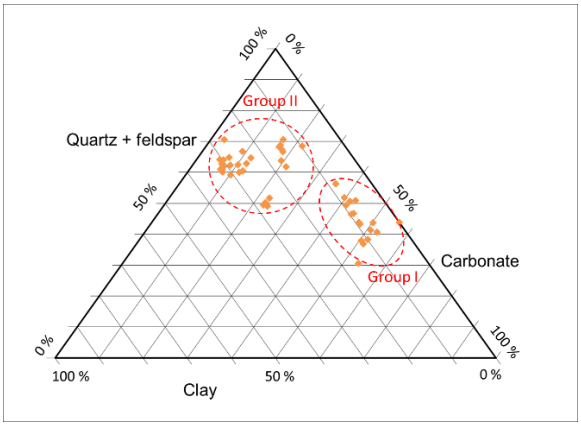

Figure 10. Ternary plot of distributions of quartz + felspar, carbonate and clay

According to the different characteristics of minerals, the seven minerals except pyrite can be divided into three major categories: 1) quartz + feldspar including albite, orthoclase and quartz; 2) carbonate including calcite and dolomite; 3) clay including muscovite/illite and chlorite. The ternary plot shows distributions of three mineral groups at all test locations in Figure 10.

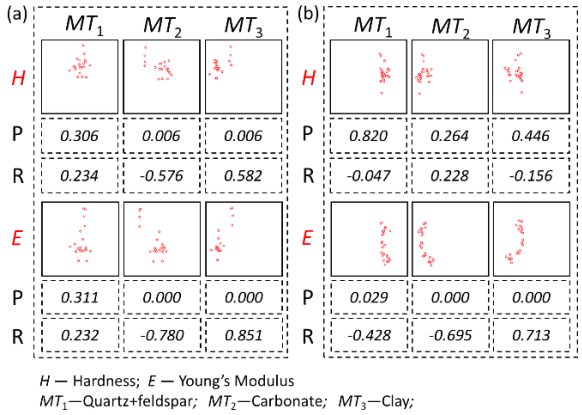

Figure 11. Scatter plot of mechanical properties and mineral types and their P and R values for (a) group I and (b) group II sample sets outlined in Figure 10.

From the ternary plot, the types of mineral compositions can be divided into two groups. Group I comprises a high content of quartz (40%-50%) and carbonate (40%-50%), and low content of clay (10%). Group II comprises high content of quartz (50%-70%), medium content of carbonate (30%-40%) and low content of clay (10%-30%). We analyzed the correlation between three mineral types and mechanical properties separately for these two groups. The result is shown in Figure 11.

There is no significant correlation between quartz + feldspar and hardness for both parts. This may be due to the low coefficient of deviation of quartz + felspar (0.18) data, and the effect of quartz can not be shown in this data set. For group I, carbonate has a negative correlation and clay has a positive correlation with hardness. When the quartz + felspar is the dominant mineral type (group II), the other two mineral types have no significant correlation with hardness. This phenomenon shows the potential effect of quartz + felspar on hardness.

Young's modulus has a negative correlation with quartz + felspar in group I, whereas it has a negative correlation with carbonate and a positive correlation with clay in both groups. This result also can be shown from the scatter charts, as data points show a downward trend of Young's modulus with an increase in carbonate, whereas points have an upward trend of Young's modulus with an increase in clay. One of the possible reasons is that carbonate, especially dolomite, is highly porous compared with clay minerals, as observed from SEM images.

5 CONCLUSION

Mineral compositions were calculated by the least-square method from the XRF data and compared with the XRD measurements. The result shows the excellent consistency with both data, which indicates the feasibility of the least-square method as an analysis tool to determine localized mineral compositions.

The correlations between chemical elements and localized mechanical properties were analyzed. Ca is negatively related to Young's modulus and Al is positively related to Young's modulus. Moreover, the correlation between minerals and localized mechanical properties was also analyzed. There is a positive correlation between hardness and albite. But two minerals, calcite and quartz, have a negative correlation with Young's modulus. Meanwhile, the correlation coefficient of chemical elements and minerals has well corresponded.

Moreover, the result shows that quartz + felspar has the potential controlling effect on hardness together with other minerals. The interpretation of the localized micro-indentation results indicates that carbonates have a negative correlation with hardness and Young's modulus, whereas clay minerals have a positive correlation with hardness and Young's modulus for the test samples.

It should be noted that the results presented here are preliminary, and work is ongoing to comprehensively understand the influence of mineral characteristics on their mechanical behaviours.

6 REFERENCES

Akkaş, E., Akin, L., Evren Çubukçu, H., and Artuner, H. (2015). Application of Decision Tree Algorithm for classification and identification of natural minerals using SEM–EDS. *Computers & Geosciences, 80*: 38-48.

British Columbia Oil and Gas Commission (2013) https://files.bcogc.ca/. Accessed 12 December 2021.

Cheng, P., Zhang, C. P., Ma, Z. Y., Zhou, J. P., Zhang, D. C., Liu, X. F., et al. (2022). Experimental study of micromechanical properties alterations of shale matrix treated by ScCO2-Water saturation using nanoindentation tests. *Energy, 242*.

Fandrich, R., Gu, Y., Burrows, D., and Moeller, K. (2007). Modern SEM-based mineral liberation analysis. *International Journal of Mineral Processing, 84*(1-4): 310-320.

Kasyap, S. S., Li, S., and Senetakis, K. (2021). Investigation of the mechanical properties and the influence of micro-structural characteristics of aggregates using micro-indentation and Weibull analysis. *Construction and Building Materials, 271*.

Meyer, M. C., Austin, P., and Tropper, P. (2013). Quantitative evaluation of mineral grains using automated SEM–EDS analysis and its application potential in optically stimulated luminescence dating. *Radiation Measurements, 58*: 1-11.

Oliver, W. C., and Pharr, G. M. (2004). Measurement of hardness and elastic modulus by instrumented indentation: Advances in understanding and refinements to methodology. *Journal of materials research, 19*(1): 3-20.

Poon, B., Rittel, D., and Ravichandran, G. (2008). An analysis of nanoindentation in linearly elastic solids. *International Journal of Solids and Structures, 45*(24): 6018-6033.

Rivard, C., Lavoie, D., Lefebvre, R., Séjourné, S., Lamontagne, C., and Duchesne, M. (2014). An overview of Canadian shale gas production and environmental concerns. *International Journal of Coal Geology, 126*: 64-76.

Sharma, P., Prakash, R., and Abedi, S. (2019). Effect of temperature on nano- and microscale creep properties of organic-rich shales. *Journal of Petroleum Science and Engineering, 175*: 375-388.

Song, J., Xiang, D., Hu, D., Zhou, H., Guo, D., and Zhang, G. (2022). Creep characteristics of a fracturing fluid-softened shale investigated by microindentation. *International Journal of Rock Mechanics and Mining Sciences, 152*.

Vishkai, M., Wang, J., Wong, R. C. K., Clarkson, C. R., and Gates, I. D. (2017). Modeling geomechanical properties in the montney formation, Alberta, Canada. *International Journal of Rock Mechanics and Mining Sciences, 96*: 94-105.

Zheng, W., Tannant, D. D., Cui, X., Xu, C., and Hu, X. (2019). Improved discrete element modeling for proppant embedment into rock surfaces. *Acta Geotechnica, 15*(2): 347-364.